

# Quantitative Analysis on the Impact of Geometry on Results of the Simulation of Blood Flow

**M. Razzaq · J. Acker · S. Turek · J.**

**Hron · F. Weichert · L. Walczak · H.**

**Müller · M. Wagner · C. Roth · F.**

**Ahlhelm · G. Schulte-Altendorneburg · I.**

**Grunwald · B. Romeike**

the date of receipt and acceptance should be inserted later

---

Mudassar Razzaq, Jens F. Acker, Stefan Turek, Jaroslav Hron

Institute of Applied Mathematics, LS III, University of Technology Dortmund, Germany

Frank Weichert, Lars Walczak, Heinrich Müller

Department of Computer Science VII, University of Technology Dortmund, Germany

Tel.: +49-231-755-6122, Fax: +49-231-755-6321,

E-mail: frank.weichert@tu-dortmund.de

Mathias Wagner

Department of Pathology, Saar State University, Homburg Campus, School of Medicine,  
Germany

Christian Roth, Frank Ahlhelm, Gernot Schulte-Altendorneburg, Iris Q. Grunwald

Clinic for Diagnostic and Interventional Neuroradiology, Saar State University, Homburg  
Campus, School of Medicine, Germany

Bernd F. M. Romeike

Department of Neuropathology, Friedrich-Schiller-University, Jena, Germany

**Abstract** Occlusion performance of sole endoluminal stenting of intracranial aneurysms is controversially discussed in literature. Simulation of blood flow have been studied to shed light on possible causal attributions. The outcome however largely depends on the degree of accuracy of geometry representation as provided by the means of segmentation. The current study was therefore conducted to learn more about the impact of segmentation artifacts on the results of Computational Fluid Dynamics (CFD). The 2D architecture of the intracranial aneurysm was based on histology. CFD was applied to assess flow and aneurysmal vorticity. As expected, the quality of the input determines the quality of the output. Stent design alone can diminish or at least has considerable influence on blood flow into the lesion. The amount of inaccuracy that is acceptable may correlate with the size of the database and properties of its application.

**Keywords** Simulation of Blood Flow · Aneurysm · Segmentation · Histology · CFD

## 1 Introduction

Hemorrhage as a consequence of ruptured intracranial aneurysms can be prevented by the means of minimally invasive therapy, endoluminal stenting. Quantitative approaches however applied to learn more about how specific design features of endovascular stents such as porosity Aenis et al (1997), struts Lieber et al (2002) and mesh design Liou et al (2004) affect intra-aneurysmal hemodynamics have mainly provided inconsistent results Kim et al (2008).

In some cases, stenting alone has been suggested to promote thrombogenic conditions such as reduced flow activity and prolonged stasis, and thereby occlude aneurysms simply by thrombosis. The present study has therefore been conducted to generate a mathematical model to evaluate this concept.

The paper is organized as follows: section 2.1 describes the animal experimentation and the preparation, resulting in a set of histological slides. Section 2.2 addresses the approach to provide a set of polygons representing the segmentation. Based on the given segmentation a simulation of the blood flow is applied to analyze the behavior of the aneurysm (cf. section 2.4). Analysis results of different example settings with varying conditions are discussed in section 2.5.

## **2 Materials and Methods**

### **2.1 Animal Experimentation**

Details on animal experimentation and sample preparation have been described previously in Ahlhelm et al (2007); Romeike and Feiden (1998). In brief, an intracerebral aneurysm has been induced in a male New Zealand White Rabbit (species: *Oryctolagus cuniculus*; National Center for Biotechnology Information Taxonomy ID: 9986 Wheeler et al (2000); average body weight as a response on a standard laboratory diet: 3.000 – 4.000g.

---

Anaesthesia was induced using an intramuscular injection of dl 2-(o-chlorophenyl)-2-(methylamino)cyclohexanone hydrochloride (syn.: ketamine hydrochloride; CAS No: 96448 – 41 – 8; *KetaVet*<sup>®</sup>; Vedco Inc., St Joseph, MO, USA; dose: 60 mg per kg body weight) and 2-(2,6-Dimethylphenylamino)-4H-5,6-dihydro-1,3-thiazine hydrochloride (xylazine hydrochloride; CAS: 7361 – 61 – 7; *Tranquived*<sup>®</sup>; Vedco, 6 mg per kg body weight). Maintenance was conducted using a mixture of the two diluted in 10ml sodium chloride (saline; CAS: 8028 – 77 – 1) which was administered by continuous intravenous infusion (mean flow-rate of 5.5 ml per hour) through the ear vein. The authors removed the fur at the neck and disinfected the site of intervention. The right common carotid artery was surgically exposed over a stretch of  $\sim 2$  cm, and its cranial part was ligated permanently with a 3-0 polyester suture (*Ethibond*<sup>®</sup>; Ethicon, Inc., Somerville, NJ, USA) prior to arteriotomy. After fixation of an intraluminal sheath (Cordis Corp., Miami Lakes, FL, USA), a 3-French balloon catheter (*Fogarty*<sup>®</sup>; Baxter Healthcare Corp., Irvine, CA, USA) was advanced to the origin of the right common carotid artery (CCA) in the brachiocephalic trunk under radioscopic guidance. A mixture of 50/50 saline (0.9%) and non-ionic radiographic contrast medium (*Omnipaque 300*<sup>®</sup>; Nycomed Amersham Imaging, Princeton, NJ, USA) was used for inflation. A *Prowler 10*<sup>®</sup> microcatheter (Cordis Corp.) was placed up-stream the inflated balloon to inject 100 U of porcine elastase (EC 3.4.21.36; Sigma Aldrich Chemie GmbH, Schnellendorf, FRG; intravascular incubation period: 20 min). Removal of the balloon catheter, microcatheter and sheath was followed by

---

the ligation of the CCA a few centimeters down-stream the brachiocephalic trunc to form the aneurysmal sac. Wounds were closed with either sutures or liquid skin adhesive (*Dermabond*<sup>®</sup>; Ethicon, Inc.). As a pilot study revealed that a considerable increase in aneurysm size appears to be rather unlikely 3-6 weeks after induction (data not shown), the authors did not perform venous control angiograms during this post-operative period.

Stenting was performed 6 weeks after aneurysm induction. The animal was therefore anaesthetized again according to the protocol described above. The right femoral artery was surgically exposed and distally ligated. A 6-French sheath was introduced into the vessel subsequent to arteriotomy and fixated with a suture. The animal was given 1.000 IE of heparin intravenously when an *Enterprise*<sup>®</sup> stent (Cordis Corp.) was placed over the neck of the aneurysm. A control angiogram was conducted immediately to visualize a possible instant occlusion of the aneurysm. The wound was closed as said above following microcatheter retrieval and ligation of the femoral artery.

The aforementioned anaesthesiological procedures were carried out to allow venous and arterial control angiographies 3 months after the first intervention. A 22 gauge *Optiva 2*<sup>®</sup> cannula (Medex Medical GmbH & CO. KG, Wallisellen, CH) was therefore placed in the left ear vein to inject a bolus of 6 – 7 ml of *Omnipaque 300* followed by 6 – 7 ml saline. Digital subtraction imaging was conducted at a rate of 2 frames per second. The animal was then sacrificed

using pentobarbital sodium (*Narcofen*<sup>®</sup>, Merial GmbH, Halbergmoos, FRG). The aortic arch as well as the proximal great vessels with the aneurysm were subsequently exposed at thoracotomy and dissected from the surrounding mediastinum.

## 2.2 Histologic Evaluation

The aneurysm was fixed in 3% neutral buffered formalin at room temperature. The specimen was subjected to a methanol-mediated dehydration period of 2 hours which was followed by the admixture of a composition of 250 ml methyl methacrylate (CAS: 80 – 62 – 6; Merck KG aA, Darmstadt, FRG), 8.75 g alpha,alpha'-azoisobutyronitrile (CAS: 78-67-1; Boehringer Ingelheim Pharma GmbH & CO KG, Heidelberg, FRG) and 62.5 g nonylphenyl-polyethylene glycol (*Nonidet*<sup>®</sup> P40; CAS: 9016 – 45 – 9; Fluka Chemie AG, Neu-Ulm, FRG) which was renewed every 30 minutes. Airtight sealing was provided by Kisol isolation foil (Kettenbach GmbH & CO KG, Eschenburg-Eibelshausen, FRG). Immersion took place in an exsiccator for about 6 hours at room temperature. The material was placed in a water bath at 351°C to facilitate the initialization of polymerization. An increment in temperature of 1°C per day was imposed to harden the composition appropriately. The polymer blocks were iteratively trimmed using the *ISOMET 2000*<sup>®</sup> precision saw (Buehler GmbH, Düsseldorf, FRG) and the rotating grinding and polishing machine DP U4 (Struers A/S, Ballerup, DK). At a thickness of approximately 5 – 10µm, the slides were stained with toluidine blue (CAS: 92 – 31 – 9; Carl Roth GmbH & CO KG,



**Fig. 1** Histologic sample shows the segmentation of the lumen of aneurysm and the structure of the stent.

Karlsruhe, FRG) after adhesion to acrylic carriers (Cadillac Plastic GmbH, Düsseldorf, FRG).

### 2.3 Acquisition and Segmentation

Digital photographs of the aneurysm were obtained at a magnification of 20X using a DP71 digital camera mounted onto a BX40 microscope (Olympus Optical CO, LTD) (cf. fig. 1).

Geometrical boundaries of the blood vessel walls including the aneurysm were assigned within the pictures by the means of manual segmentation using the prototypical software SeViSe Landes et al (2005) so that the positions of the markers that were attributed to these structures coincided with the outlines of the 2D object as accurately as possible. In order to rule out bias when op-

erated single-handedly by one histopathologist, a total of three independent examiners performed manual segmentation.

In order to reduce the number of control points of the polygons, in consequence reducing the dimension of the mesh for the blood flow, the Douglas Peucker divide-and-conquer algorithm was applied Douglas and Peucker (1973). For the given data set, the reduction was applied to reduce the control points count mainly of the inner layer of the vessel wall and the outer layer of the vessel wall. It simplifies the polygon by removing control points, that do not contribute enough (given a parameter  $\epsilon$ ) to the polygons shape, without modifying the fundamental appearance and the underlying anatomical information. A simplification with  $\epsilon = 0.1$  pixel means a subpixel precision, so practically only the co-linear control points would be filtered out. This caused a reduction for the inner Wall from 2527 to 1406 points (55,6%) and for the outer Wall from 1640 to 1031 (62.8%) points. The average deviation to the old polygon was, as expected through the elimination of only co-linear points, in both cases equal as good as 0 pixels (0.021 resp. 0.016). After applying the reduction with  $\epsilon = 1$ , which means the reduction of nearly co-linear segments, the vertices count dropped to 388 (15.3%) for the inner Wall respectively 338 (20.6%) for the outer Wall.

---

## 2.4 Simulation of Blood Flow

There have been several different approaches to the problem of fluid-structure interaction in blood flow dynamics in local arterial environments and to predict vessel wall deformation. In Steinman et al (2003) image based computational simulation of the flow dynamics (CFD) is reported for Newtonian fluid in a giant cerebral aneurysm. In Cebal et al (2005b) a clinical study in which the association between intra-aneurysm hemodynamic characteristics from CFD models described and the rupture of cerebral aneurysms was investigated. A sensitivity analysis of the hemodynamic characteristics with respect to variations involving several variables in patient specific models of cerebral aneurysms presented in Cebal et al (2005a); they found that the variable that had the greatest effect on the flow field was the vessel geometry. In reality the thickness of the wall can be significant and very important and it is very hard to predict material property of wall thickness. For example in arteries the wall thickness can be up to 30% of the diameter and its local thickening can be the cause of an aneurysm creation. A coupled monolithic FSI (fluid-structure interaction) modeling approach is developed and efficiently implemented to this complex problem.

### *2.4.1 Modeling Hemodynamics*

Modeling FSI in the blood circulatory system is a vast and complex mathematical subject. The general fluid-structure interaction problem consists of the description of the fluid and structure fields, appropriate interface conditions

at the interface and conditions for the remaining boundaries, respectively. We denote the domain occupied by the fluid (blood) by  $\Omega_t^f$  and the structure (blood vessel elastic walls) by  $\Omega_t^s$  at the time  $t \in [0, T]$ . Let  $\Gamma_t^0 = \bar{\Omega}_t^f \cap \bar{\Omega}_t^s$  be the part of the boundary where blood interacts with the blood vessel elastic walls. The governing equations for fluid and structure are derived in the ALE framework. we assume blood to be incompressible Newtonian governed by the Navier-Stokes equations

$$\rho^f \left( \frac{\partial \mathbf{v}^f}{\partial t} + \mathbf{v}^f \cdot \nabla \mathbf{v}^f \right) - \nabla \cdot \boldsymbol{\sigma}^f = \mathbf{0}, \quad \nabla \cdot \mathbf{v}^f = \mathbf{0} \quad \text{in } \Omega_t^f \quad (1)$$

where  $\rho^f$  is the constant density and  $\mathbf{v}^f$  is the velocity of the fluid. The constitutive relations for the stress tensors read

$$\boldsymbol{\sigma}^f = -p^f \mathbf{I} + 2\mu \boldsymbol{\varepsilon}(\mathbf{v}^f), \quad (2)$$

where  $\mu$  is the dynamic viscosity of the fluid,  $p^f$  is the Lagrange multiplier corresponding to the incompressibility constraint in (1), and  $\boldsymbol{\varepsilon}(\mathbf{v}^f)$  is the strain-rate tensor:

$$\boldsymbol{\varepsilon}(\mathbf{v}^f) = \frac{1}{2} (\nabla \mathbf{v}^f + (\nabla \mathbf{v}^f)^T). \quad (3)$$

We considered the effects of a non-Newtonian fluid model on hemodynamics. The Carreau fluid model was selected because it is an accurate model to describe the rheological behavior of blood Johnston et al (2004). Experimental tests show that blood exhibits shear thinning apart of other non-Newtonian phenomena. Thus, in order to include this feature the viscosity in the following

form is used

$$\mu(|\mathbf{D}(\mathbf{v})|) = \mu_\infty + (\mu_0 - \mu_\infty)(1 + K|\mathbf{D}(\mathbf{v})|^2)^n. \quad (4)$$

The Carreau blood model predicts decreasing viscosity at high strain, where  $\mu_0$  and  $\mu_\infty$  are low and high shear rate asymptotic values, and parameters  $K$  and  $n$  control the transition region. We have taken the parameter values as  $\mu_\infty = 0.00345 \text{Ns/m}^2$ ,  $\mu_0 = 0.056 \text{Ns/m}^2$ ,  $K = 10.976$   $n = -0.3216$

The governing equations for the structure in the more common Lagrangian description, i.e. with respect to some fixed reference (initial) state  $\Omega^s$ :

$$\rho^s \left( \frac{\partial^2 \mathbf{u}^s}{\partial t^2} - \mathbf{g}^s \right) - \nabla \cdot \Sigma^s = \mathbf{0}, \quad \text{in } \Omega^s, \quad (5)$$

where the subscript  $s$  denotes the structure,  $\rho^s$  is the density of the structure,  $\mathbf{g}^s$  represents the external body forces acting on the structure. The configuration of the structure is described by the displacement  $\mathbf{u}^s$ , with velocity field  $\mathbf{v}^s = \frac{\partial \mathbf{u}^s}{\partial t}$ , where the tensor  $\Sigma^s = J \sigma^s \mathbf{F}^{-T}$  is the non-symmetric first Piola-Kirchhoff tensor and  $\sigma^s$  is the Cauchy stress tensor. It is natural to introduce the symmetric second Piola-Kirchhoff tensor  $\mathbf{S}^s$  in this case

$$\mathbf{S}^s = \mathbf{F}^{-T} \Sigma^s = J \mathbf{F}^{-1} \sigma^s \mathbf{F}^{-T}, \quad (6)$$

we suppose elastic blood vessel walls to be linear, for which, mechanically homogeneous isotropic material is usually written in terms of the Green-Lagrange strain tensor, as

$$\mathbf{E} = \frac{1}{2}(\mathbf{C} - \mathbf{I}), \quad (7)$$

where  $\mathbf{I}$  is the identity tensor and  $\mathbf{C} = \mathbf{F}^T \mathbf{F}$  is the right Cauchy-Green strain tensor.  $J$  denotes the determinant of the deformation gradient tensor  $\mathbf{F}$ , defined as  $\mathbf{F} = \mathbf{I} + \nabla \mathbf{u}^s$ .

For this hemodynamic applications, a Neo-Hooke material model ( $J = \det \mathbf{F}$ ) is taken which can be used for compressible or incompressible (for  $\nu^s = 1/2 \Rightarrow \lambda^s \rightarrow \infty$ ) material and which is described by the constitutive laws

$$\boldsymbol{\sigma}^s = -p^s \mathbf{I} + \frac{\mu^s}{J} (\mathbf{F} \mathbf{F}^T - \mathbf{I}) \quad (8)$$

$$\mathbf{0} = -p^s + \frac{\lambda^s}{2} \left( J - \frac{1}{J} \right) \quad (9)$$

The Neo-Hooke material model is isotropic and hyperelastic, and can be used for the computation of large deformations. The results for a given set of Young modulus  $E$  and poisson ratio  $\nu^s$  or lamé coefficients  $\lambda^s$  and shear modulus  $\mu^s$  are comparable for the standard Neo-Hooke material model as in (9) is used. Aneurysms walls can exhibit anisotropic behavior in the case of more complex blood flow. In this case more realistic constitutive relations can be comprehended which however is not discussed here.

#### 2.4.2 Interaction conditions

The boundary conditions on the blood-vessel wall interface are assumed to be

$$\boldsymbol{\sigma}^f n = \boldsymbol{\sigma}^s n, \quad \mathbf{v}^f = \mathbf{v}^s, \quad \text{on } \Gamma_t^0, \quad (10)$$

where  $n$  is a unit normal vector to the interface  $\Gamma_t^0$ . This implies the no-slip condition for the flow and that the forces on the interface are in balance.

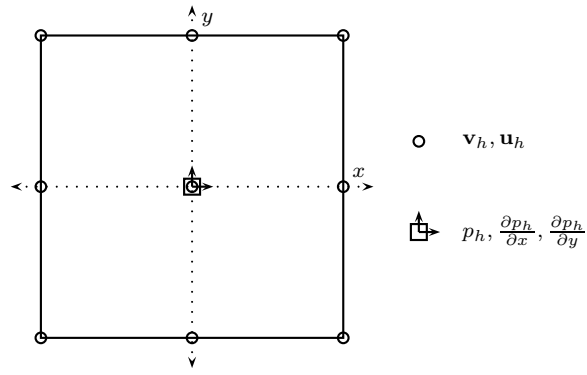


**Fig. 2** Location of the degrees of freedom for the  $Q_2P_1$  element.

### 2.4.3 Discretization and solution techniques

In this study, we restrict at the moment to two dimensions which allows systematic tests of the proposed methods for biomedical applications in a very efficient way such that the qualitative behaviour can be carefully analyzed. The corresponding fully implicit, monolithic treatment of the fluid-structure interaction problem suggests that an A-stable second order time stepping scheme and that the same finite elements for both the solid part and the fluid region should be utilized. Moreover, to circumvent the fluid incompressibility constraints, we have to choose a stable finite element pair. For that reason, the conforming biquadratic, discontinuous bilinear  $Q_2P_1$  pair, see Figure 2 for the location of the degrees of freedom, is chosen which is explained in Razzaq et al (2009) in detail.

#### 2.4.4 Numerical solutions

Mostly, in literature solution strategy used is to decouple the problem into the fluid part and structure part, for each of those parts to use some well established method of solution and the interaction is introduced as external boundary conditions or volume forces in each of the subproblems. This has a great advantage that there are many well tested finite element based numerical methods for separate problems of fluid flow and elastic deformation, on the other hand the treatment of the interface and the interaction is problematic. An Arbitrary Lagrangian-Eulerian (ALE) formulation is employed in a fully coupled monolithic way, considering the problem as one continuum. After applying the standard finite element method with the  $Q_2P_1$  element pair. The system of nonlinear algebraic equations arising from the governing equations reads

$$\begin{pmatrix} S_{\mathbf{u}\mathbf{u}} & S_{\mathbf{u}\mathbf{v}} & 0 \\ S_{\mathbf{v}\mathbf{u}} & S_{\mathbf{v}\mathbf{v}} & kB \\ c_{\mathbf{u}}B_s^T & c_{\mathbf{v}}B_f^T & 0 \end{pmatrix} \begin{pmatrix} \mathbf{u} \\ \mathbf{v} \\ p \end{pmatrix} = \begin{pmatrix} \mathbf{f}_{\mathbf{u}} \\ \mathbf{f}_{\mathbf{v}} \\ f_p \end{pmatrix}, \quad (11)$$

which is a typical saddle point problem, where  $S$  describes the diffusive and convective terms from the governing equations. The above system of nonlinear algebraic equations (11) is solved using Newton method as basic iteration which can exhibit quadratic convergence provided that the initial guess is sufficiently close to the solution. The basic idea of the Newton iteration is to find a root of a function,  $\mathbf{R}(\mathbf{X}) = \mathbf{0}$ , using the available known function value

and its first derivative, One step of the Newton iteration can be written as

$$\mathbf{X}^{n+1} = \mathbf{X}^n + \omega^n \left[ \frac{\partial \mathbf{R}(\mathbf{X}^n)}{\partial \mathbf{X}} \right]^{-1} \mathbf{R}(\mathbf{X}^n), \quad (12)$$

where  $\mathbf{X} = (\mathbf{u}_h, \mathbf{v}_h, p_h)$ . The dumped Newton method with line search improves the chance of convergence by adaptively changing the length of the correction vector. The solution update step in the Newton method (12) is replaced by

$$\mathbf{X}^{n+1} = \mathbf{X}^n + \omega \delta \mathbf{X}, \quad (13)$$

where the parameter  $\omega$  is found such that certain error measure decreases.

One of the possible choices for the quantity to decrease is

$$f(\omega) = \mathcal{F}(\mathbf{X}^n + \omega \delta \mathbf{X}) \cdot \delta \mathbf{X}. \quad (14)$$

Since we know

$$f(0) = \mathcal{F}(\mathbf{X}^n) \cdot \delta \mathbf{X}, \quad (15)$$

and

$$f'(0) = \left[ \frac{\partial \mathcal{F}}{\partial \mathbf{X}}(\mathbf{X}^n) \right] \delta \mathbf{X} \cdot \delta \mathbf{X} = \mathcal{F}(\mathbf{X}^n) \cdot \delta \mathbf{X}, \quad (16)$$

and computing  $f(\omega_0)$  for  $\omega_0 = -1$  or  $\omega_0$  determined adaptively from previous iterations we can approximate  $f(\omega)$  by a quadratic function

$$f(\omega) = \frac{f(\omega_0) - f(0)(\omega_0 + 1)}{\omega_0^2} \omega^2 + f(0)(\omega + 1). \quad (17)$$

Then setting

$$\tilde{\omega} = \frac{f(0)\omega_0^2}{f(\omega_0) - f(0)(\omega_0 + 1)}, \quad (18)$$

the new optimal step length  $\omega \in [-1, 0]$  is

$$\omega = \begin{cases} -\frac{\tilde{\omega}}{2} & \text{if } \frac{f(0)}{f(\omega_0)} > 0, \\ -\frac{\tilde{\omega}}{2} - \sqrt{\frac{\tilde{\omega}^2}{4} - \tilde{\omega}} & \text{if } \frac{f(0)}{f(\omega_0)} \leq 0. \end{cases} \quad (19)$$

This line search can be repeated with  $\omega_0$  taken as the last  $\omega$  until, for example,  $f(\omega) \leq \frac{1}{2}f(0)$ . By this we can enforce a monotonous convergence of the approximation  $\mathbf{X}^n$ . The Jacobian matrix  $\frac{\partial \mathbf{R}(\mathbf{X}^n)}{\partial \mathbf{X}}$  can be computed by finite

- 
1. Let  $\mathbf{X}^n$  be some starting guess.
  2. Set the residuum vector  $\mathbf{R}^n = \mathcal{F}(\mathbf{X}^n)$  and the tangent matrix  $\mathbf{A} = \frac{\partial \mathcal{F}}{\partial \mathbf{X}}(\mathbf{X}^n)$ .
  3. Solve for the correction  $\delta \mathbf{X}$ 

$$\mathbf{A} \delta \mathbf{X} = \mathbf{R}^n.$$
  4. Find optimal step length  $\omega$ .
  5. Update the solution  $\mathbf{X}^{n+1} = \mathbf{X}^n - \omega \delta \mathbf{X}$ .
- 

**Fig. 3** One step of the Newton method with the line search.

differences from the residual vector  $\mathbf{R}(\mathbf{X})$

$$\left[ \frac{\partial \mathbf{R}(\mathbf{X}^n)}{\partial \mathbf{X}} \right]_{ij} \approx \frac{[\mathbf{R}]_i(\mathbf{X}^n + \alpha_j \mathbf{e}_j) - [\mathbf{R}]_i(\mathbf{X}^n - \alpha_j \mathbf{e}_j)}{2\alpha_j}, \quad (20)$$

where  $\mathbf{e}_j$  are the unit basis vectors in  $\mathbf{R}^n$  and the coefficients  $\alpha_j$  are adaptively taken according to the change in the solution in the previous time step. Since we know the sparsity pattern of the Jacobian matrix in advance, which is given by the used finite element method, this computation can be done in an efficient way so that the linear solver remains the dominant part in terms of the CPU time (see Turek (1999); Turek and Schmachtel (2002) for more details). A good candidate, at least in 2D, seems to be a direct solver for sparse systems

like UMFPACK (see Davis and Duff (1999)); while this choice provides very robust linear solvers, its memory and CPU time requirements are too high for larger systems (i.e. more than 20.000 unknowns). Large linear problems can be solved by Krylov-space methods (BiCGStab, GMRes, see Barrett et al (PA 1994)) with suitable preconditioners. One possibility is the ILU preconditioner with special treatment of the saddle point character of our system, where we allow certain fill-in for the zero diagonal blocks, see Bramley and Wang (1997). As an alternative, we also utilize a standard geometric multigrid approach based on a hierarchy of grids obtained by successive regular refinement of a given coarse mesh. The complete multigrid iteration is performed in the standard defect-correction setup with the V or F-type cycle. While a direct sparse solver Davis and Duff (1999) is used for the coarse grid solution, on finer levels a fixed number (2 or 4) of iterations by local MPSC schemes (Vanka-like smoother) Turek (1999); Vanka (1985); Hron and Turek (2006) is performed. Such iterations can be written as

$$\begin{pmatrix} \mathbf{u}^{l+1} \\ \mathbf{v}^{l+1} \\ p^{l+1} \end{pmatrix} = \begin{pmatrix} \mathbf{u}^l \\ \mathbf{v}^l \\ p^l \end{pmatrix} - \omega \sum_{\text{element } \Omega_i} \begin{pmatrix} S_{\mathbf{uu}|\Omega_i} & S_{\mathbf{uv}|\Omega_i} & 0 \\ S_{\mathbf{vu}|\Omega_i} & S_{\mathbf{vv}|\Omega_i} & kB_{|\Omega_i} \\ c_{\mathbf{u}}B_{s|\Omega_i}^T & c_{\mathbf{v}}B_{f|\Omega_i}^T & 0 \end{pmatrix}^{-1} \begin{pmatrix} \mathbf{def}_{\mathbf{u}}^l \\ \mathbf{def}_{\mathbf{v}}^l \\ def_p^l \end{pmatrix}.$$

The inverse of the local systems ( $39 \times 39$ ) can be done by hardware optimized direct solvers. The full nodal interpolation is used as the prolongation operator  $\mathbf{P}$  with its transposed operator used as the restriction  $\mathbf{R} = \mathbf{P}^T$  (see Hron et al (2002); Turek (1999) for more details).

### 2.4.5 Applications to hemodynamics

The aim of numerical simulations is to relate the aneurysm state (unrupture or rupture) with wall pressure, wall deformation and effective wall stress. Such a relationship would provide information for the diagnosis and treatment of unrupture and rupture of an aneurysm by elucidating the risk of bleeding or rebleeding, respectively.

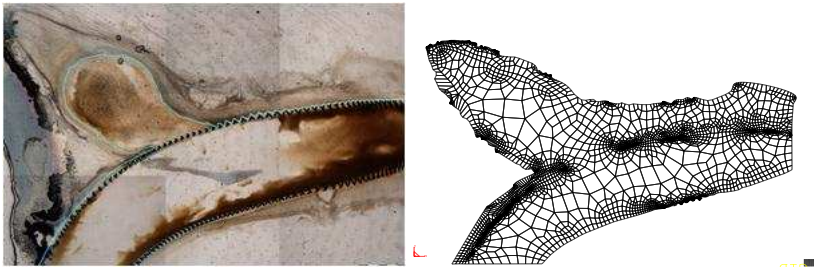


**Fig. 4** Left: Real view of aneurysm. Right: Schematic drawing of the mesh.

As a typical example for the related CFD simulations, a real view is provided in Fig. 4 which also contains the automatically extracted computational domain and (coarse) mesh in 2D, however without stents. In order to use the proposed numerical methods for aneurysm hemodynamics, in a first step, only simplified two-dimensional examples, which however include the interaction of the flow with the deformable material, are considered in the following. Flow through a deformable vein with elastic walls of a brain aneurysm is simulated to analyse qualitatively the described methods; here, the flow is driven by prescribing the flow velocity at the inflow section while the elastic part of the boundary is either fixed or stress-free. Both ends of the walls are fixed, and the flow is

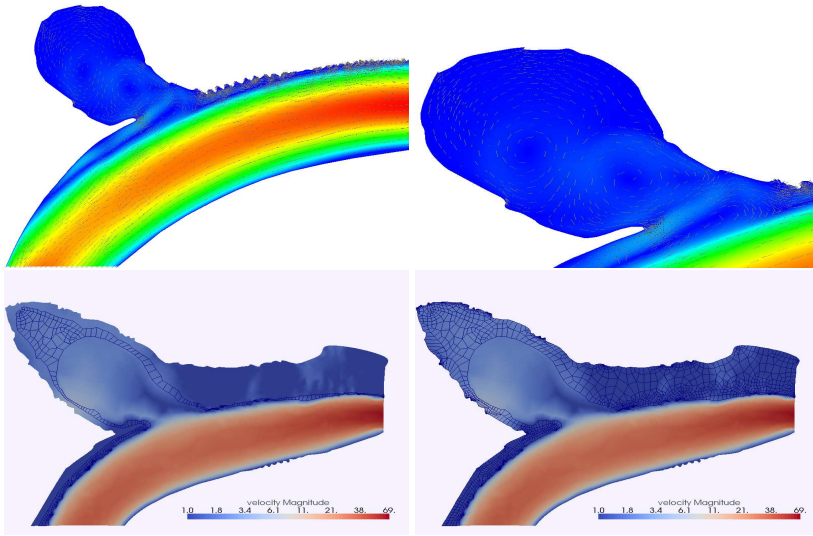


**Fig. 5** Top Left: Real view of aneurysm. Top Right: Schematic drawing of the mesh. Below Left: Thin elastic layer. Below Right: Thick elastic layer.

driven by a periodical change of the inflow at the left end. Flow pattern is seen in Fig. 5 for the Carreau fluid flow model case defined in equation 4.

#### 2.4.6 Geometry of the problem

For convenience, the geometry of the fluid domain under consideration is currently based on simplified 2D models (see Fig. 6) which allows us to concentrate on the detailed qualitative evaluation of our approach based on the described monolithic ALE formulation. The geometrical details of the shape of the aneurysm is given in the table 1 as follows (for further explanation see Razzaq et al (2008)). The examined stents are of circular shape, placed on the neck of the aneurysm, and we use three, resp., five stents (simplified ‘circles’ in 2D as cutplanes from 3D configurations) of different size and position. The

without aneurysm fundus		value [mm]
innermost circle radius	$r_1$	6
next circle radius	$r_2$	8
last circle radius	$r_3$	8.25
aneurysm fundus		value [mm]
midpoint of arcs	$C$	$(-6.75, 6)$
inner fundus radius		1.125
outer fundus radius		1.25

**Table 1** Overview of the geometry parameters.

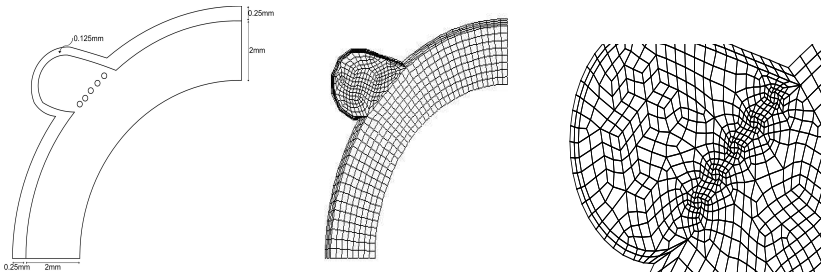


**Fig. 6** Left: Schematic drawing of the measurement section. Middle: Mesh without stents (776 elements). Right: Mesh with stents (1431 elements) which are part of the simulations.

stents also consist of a grid, immersed in the blood flow, which is located at the inlet of the aneurysm so that in future elastic deformations of the stents can be included, too, since in real life, the stent is a medical device which consists of a wire metal wire tube. Stents are typically used to keep arteries open and are located on the vessel wall while this stent is immersed in the blood flow (Fig. 6). The purpose of this device is to reduce the flux into and within the aneurysm in order to occlude it by a clot or rupture. The aneurysm

is then intersected with the blood vessel and all missing angular values and intersection points can be determined.

#### 2.4.7 Boundary and initial conditions

The (steady) velocity profile, to flow from the right to the left part of the channel, is defined as parabolic inflow, namely

$$\mathbf{v}^f(0, y) = \bar{U}(y - 6)(y - 8). \quad (21)$$

Correspondingly, the pulsatile inflow profile for the nonsteady tests for which peak systole and diastole occur for  $\Delta t = 0.25s$  and  $\Delta t = 0.75s$  respectively, is prescribed as

$$\mathbf{v}^f(t, 0, y) = \mathbf{v}^f(0, y)(1 + 0.75\sin(2\pi t)). \quad (22)$$

The natural outflow condition at the lower left part effectively prescribes some reference value for the pressure variable  $p$ , here  $p = 0$ . While this value could be arbitrarily set in the incompressible case, in the case of a compressible structure this might have influence onto the stress and consequently the deformation of the solid. The *no-slip* condition is prescribed for the fluid on the other boundary parts, i.e. top and bottom wall, stents and fluid-structure interface.

#### 2.4.8 Numerical results

As described before, the constitutive relations used for the materials are the incompressible Newtonian model (2) for the fluid and a hyperelastic Neo-Hooke material for the structure, furthermore, parameter values are given in the table

	parameter	values
density of structure	$\rho^s [10^{-6} \frac{\text{kg}}{\text{mm}^3}]$	1.12
poisson ratio	$\nu^s$	0.4
shear modulus	$\mu^s [\frac{\text{kg}}{\text{mm}^2}]$	42.85
density of fluid	$\rho^f [10^{-6} \frac{\text{kg}}{\text{mm}^3}]$	1.035
viscosity of fluid	$\nu^f [\frac{\text{mm}^2}{\text{s}}]$	3.38
velocity	$\bar{U} [\frac{\text{mm}}{\text{s}}]$	20
reynolds number	$Re$	120
Young modulus	$E [\frac{\text{kN}}{\text{mm}^2}]$	120

**Table 2** Parameter values

2. This choice includes most of the typical difficulties the numerical method has to deal with, namely the incompressibility and significant deformations. From a medical point of view, the use of stents provides an efficient treatment for managing the difficult entity of intracranial aneurysms. Here, the thickness of the aneurysm wall is attenuated and the aneurysm hemodynamics changes significantly. Since the purpose of this device is to control the flux within the aneurysm in order to occlude it by a clot or rupture, the resulting flow behavior into and within the aneurysm is the main objective, particularly in view of the different stent geometries. Therefore, we decided for the 2D studies to locate the stents only in direct connection to the aneurysm. In the following, we show some corresponding results for the described prototypical aneurysm geometry, first for the steady state inflow profile, followed by nonsteady tests for the pulsatile inflow, both with rigid and elastic walls, respectively.

---

#### *2.4.9 Steady configurations*

The given inflow profile is not time-dependent, and due to the low Re numbers, the flow behaviour leads to a steady state which only depends on the elasticity and the shape of the stents. Moreover, for the following simulations, we only treat the aneurysm wall as elastic structure. Then, the aneurysm undergoes some slight deformations which can hardly be seen in the following figures. However they result in a different volume of the flow domain (see Fig. 9). Particularly the influence of the number of stents onto the complete fluid flow through the channel including the aneurysm can be clearly seen. Summarizing these results for steady inflow, the simulations show that the stent implantation across the neck of the aneurysm prevents blood penetration into the aneurysm fundus. Moreover, the elastic geometrical deformation of the wall is slightly reduced by implanting the stents while the local flow behaviour inside of the aneurysm is more significantly influenced by the elastic properties of the outer wall, particularly due to different width between stents and walls of the aneurysm. In the next section, we will consider the more realistic behaviour of flow configurations with time-dependent pulsatile inflow which will be analyzed for the case of elastic behaviour of the aneurysm walls.



**Fig. 7** Deformed mesh for steady configuration without stents, with elastic wall (left). Mesh for rigid wall (right).



**Fig. 8** Deformed mesh for steady configuration with stents: 3 stents (left) and 5 stents (right).

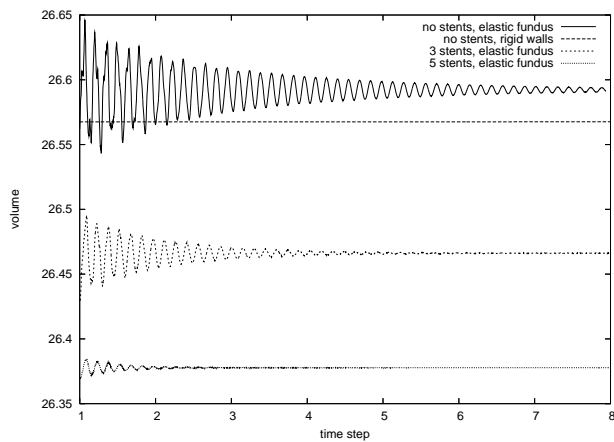


**Fig. 9** Resulting volume of the fluid domain for different configurations.

---

#### *2.4.10 Pulsatile configurations*

For the pulsatile test case, we have taken again the aneurysm part as elastic while the other parts of the walls belonging to the channel are rigid. First of all, we show again (see Fig. 10) the resulting volume of the flow domain for 5, 3 and no stents. In all cases, the oscillating behaviour due to the pulsative inflow is visible which also leads to different volume sizes. Looking carefully at the resulting flow behaviour, we see global differences w.r.t. the channel flow near the aneurysm, namely due to the different flow rate into the aneurysm, and significant local differences inside of the aneurysm.

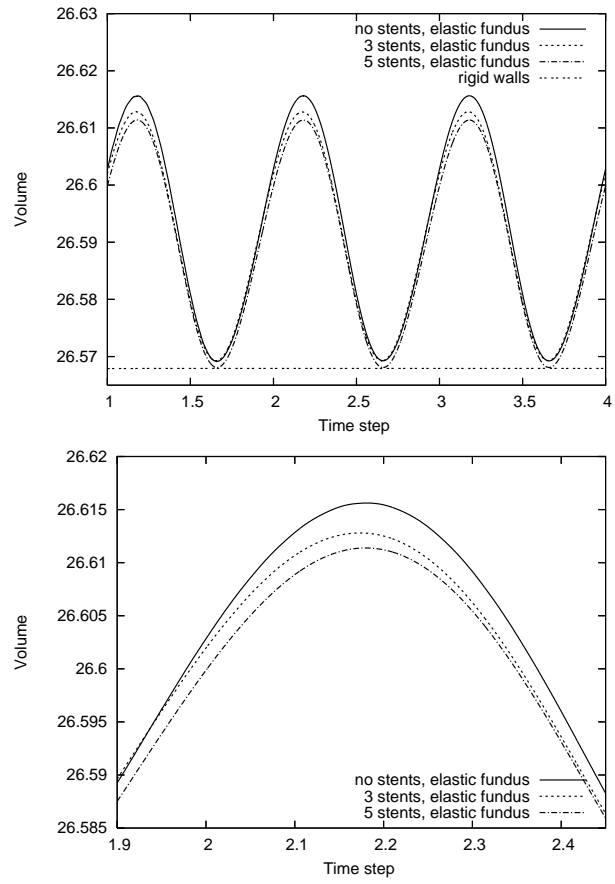
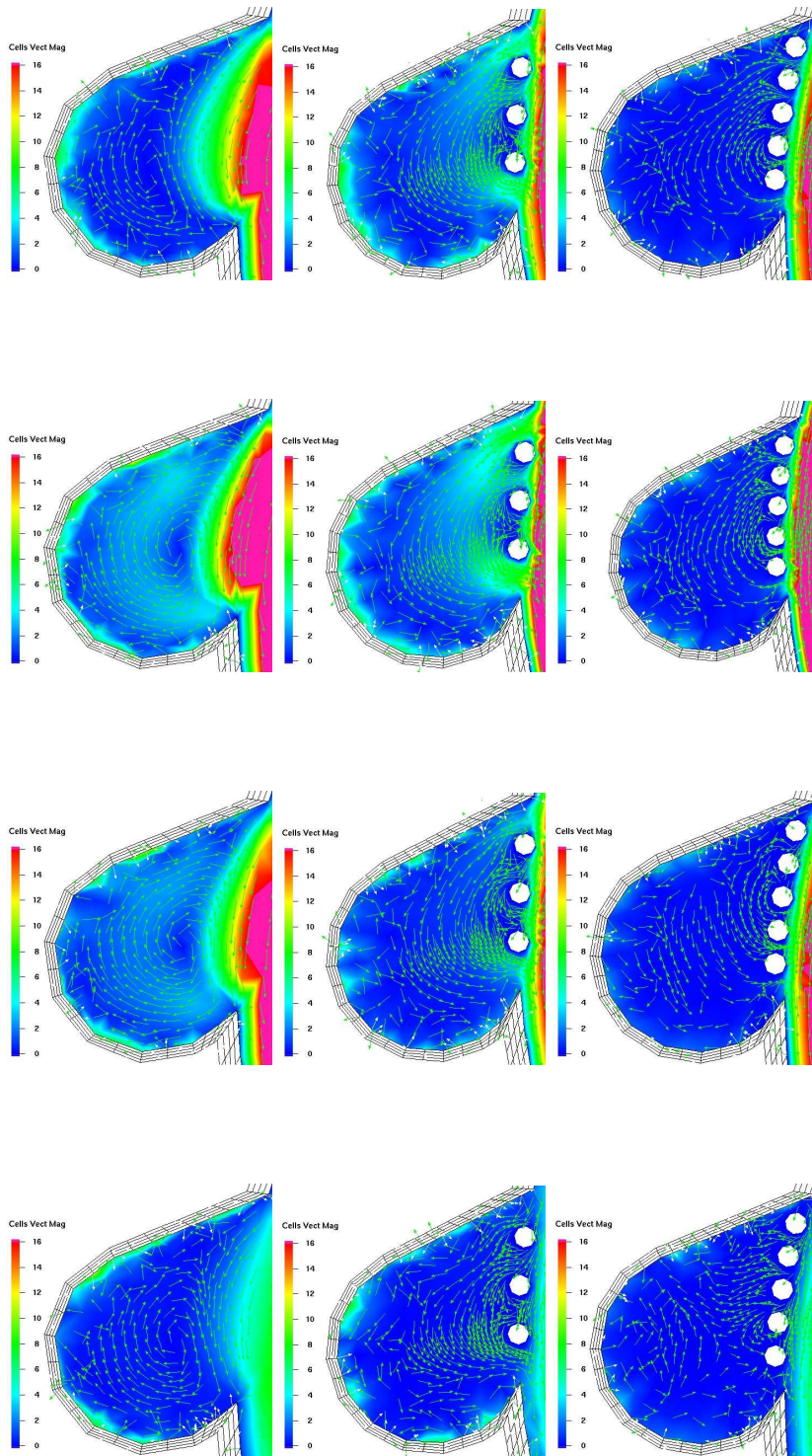


Fig. 10 Domain volume with rigid and elastic behaviour of the aneurysm wall.



**Fig. 11** Left column: no stent. Middle column: 3 stents. Right column: 5 stents. Figures demonstrate the local behaviour of the fluid flow inside of the aneurysm during one cycle.

## 2.5 Results

The animal tolerated the procedures well (the induction of the aneurysm took  $\sim 70$  minutes and the time to awakening from anesthesia was  $\sim 15$  minutes). Light microscopic histopathological work-up of the aneurysm revealed a sac filled with organized thrombotic material while myofibroblasts accrued the stent struts at the neck of the lesion and endothel-like cells covered the luminal surface of the aneurysmal aperture Ahlhelm et al (2007)

## 3 Discussion

The accuracy of CFD relies on the quality of the input. The quality of the output depends for instance on the quality of the preparation procedure for the histological slide, and on properties of the technology used for digitalization which contributes to the signal to noise ratio Landes et al (2005). It is therefore obvious that inaccurate object boundaries may alter the results of CFD.

Comparing our studies with the CFD literature (see Fernandez et al (2008); Appanaboyina et al (2008); Valencia et al (2008); Torri et al (2007a,b)), several research groups focus on CFD simulations with realistic 3D geometries, but typically assuming rigid walls. In contrast, we concentrate on the complex interaction between elastic deformations and flow perturbations induced by the stents. At the moment, we are only able to perform these simulations

---

in 2D, however, with these studies we should be able to analyse qualitatively the influence of geometrical details onto the elastic material behavior, particularly in view of more complex blood models and constitutive equations for the structure. Therefore, the aims of our current studies can be described as follows:

1. What is the influence of the elasticity of the walls onto the flow behavior inside of the aneurysm, particularly w.r.t. the resulting shape of the aneurysm?
2. What is the influence of the geometrical details of the (2D) stents, that means shape, size, position, onto the flow behavior into and inside of the aneurysm?
3. Do both aspects, small-scale geometrical details as well as elastic fluid-structure interaction, have to be considered simultaneously or is one of them negligible in first order approximation?
4. Are modern numerical methods and corresponding CFD simulations tools able to simulate qualitatively the multiphysics behavior of such biomedical configurations?

Further studies need to evaluate the applicability of this 2D approach to calculations in 3D.

**Acknowledgements** The authors want to express their gratitude to the Forschungsförderungsprogramm HOMFOR2008 for their financial support of the project.

## References

- Aenis M, Stancampiano A, Wakhloo A, Lieber B (1997) Modeling of flow in a straight stented and nonstented side wall aneurysm model. *J Biomech Eng* 119:206–212
- Ahlhelm F, Roth C, Kaufmann R, Schulte-Altendorneburg G, Romeike B, Reith W (2007) Treatment of wide-necked intracranial aneurysms with a novel self-expanding two-zonal endovascular stent device. *Neuroradiology* 49:1023–1028
- Appanaboyina S, Mut F, Löhner R, Scrivano E, Miranda C, Lylyk P, Putman C, Cebal J (2008) Computational modelling of blood flow in side arterial branches after stenting of cerebral aneurysm. *International Journal of Computational Fluid Dynamics* 22:669–676
- Barrett R, Berry M, Chan TF, Demmel J, Donato J, Dongarra J, Eijkhout V, Pozo R, Romine C, Van der Vorst H (PA 1994) *Templates for the solution of linear systems: Building blocks for iterative methods*. SIAM, Philadelphia
- Bramley R, Wang X (1997) SPLIB: A library of iterative methods for sparse linear systems. <http://www.cs.indiana.edu/ftp/bramley/splib.tar.gz>, Department of Computer Science, Indiana University, Bloomington, IN,
- Cebal JR, Castro MA, Appanaboyina S, Putman CM, Millan D, Frangi AF (2005a) Efficient pipeline for image-based patient-specific analysis of cerebral aneurysm hemodynamics : technique and sensitivity. *IEEE Transactions on Medical Imaging* 24:457–467

- 
- Cebral JR, Castro MA, Burgess JE, Pergolizzi RS, Sheridan MJ, Putman CM (2005b) Characterization of cerebral aneurysms for assessing risk of rupture by using patient-specific computational hemodynamics models. *American Journal of Neuroradiology* 26:2550–2559
- Davis TA, Duff IS (1999) A combined unifrontal/multifrontal method for unsymmetric sparse matrices. *SACM Trans Math Software* 25:1–19
- Douglas D, Peucker T (1973) Algorithms for the reduction of the number of points required to represent a digitized line or its caricature. *The Canadian Cartographer* 10(2):112–122
- Fernandez MA, Gerbeau JF, Martin V (2008) Numerical simulation of blood flows through a porous interface. *ESAIM: Mathematical Modelling and Numerical Analysis* 42:961–990
- Hron J, Turek S (2006) A monolithic FEM/multigrid solver for ALE formulation of fluid structure interaction with application in biomechanics. In: Bungartz HJ, Schäfer M (eds) *Fluid-Structure Interaction: Modelling, Simulation, Optimisation*, LNCSE:53, Springer
- Hron J, Ouazzi A, Turek S (2002) A computational comparison of two fem solvers for nonlinear incompressible flow. In: Bänsch E (ed) *Challenges in Scientific Computing*, LNCSE:53, Springer, pp 87–109
- Johnston BM, Johnston PR, Corney S, Kilpatrick D (2004) Non-newtonian blood flow in human right coronary arteries: steady state simulations. *Journal of Biomechanics* 37:709–720

- Kim M, Taulbee D, Tremmel M, Meng H (2008) Comparison of two stents in modifying cerebral aneurysm hemodynamics. *Ann Biomed Eng* 36:726–741
- Landes C, Weichert F, Geis P, Wernstedt K, Wilde A, Fritsch H, Wagner M (2005) Tissue-plastinated vs. celloidin-embedded large serial sections in video, analog and digital photographic on-screen reproduction: a preliminary step to exact virtual 3d modelling, exemplified in the normal midface and cleft-lip and palate. *J Anat* 207:175–191
- Lieber B, Livescu V, Hopkins L, Wakhloo A (2002) Particle image velocimetry assessment of stent design influence on intra-aneurysmal flow. *Ann Biomed Eng* 30:768–777
- Liou T, Liou S, Chu K (2004) Intra-aneurysmal flow with helix and mesh stent placement across side-wall aneurysm pore of a straight parent vessel. *J Biomech Eng* 126:36–43
- Razzaq M, Turek S, Hron J, Acker J, Weichert F, Wagner M, Grunwald I, Roth B Cand Romeike (2008) Numerical simulation of fluid-structure interaction with application to aneurysm hemodynamics. workshop on fluid-structure-interaction: Theory, numerics and applications herrsching am ammersee, germany. *Proc Fluid-Structure Interaction Theory, Numerics and Applications* pp 283–294
- Razzaq M, Hron J, Turek S (2009) Numerical simulation of laminar incompressible fluid-structure interaction for elastic material with point constraintst. In: Rannacher R, Sequeira A (eds) *Advances in Mathematical Fluid Mechancis-Dedicated to Giovanni paolo Galdi on the Occasion of his*

- 
- 60th Birthday, Springer, in print
- Romeike B, Feiden W (1998) Demonstration of platinum microcoils in embolized blood vessels in-situ using a modified methyl methacrylate embedding method, and a special cutting and grinding technique. *Biotech Histochem* 73:198–201
- Steinman D, Milner JS, Norley CJ, Lownie SP, W HD (2003) Image-based computational simulation of flow dynamics in a giant cerebral aneurysm. *American Journal of Neuroradiology* 24:559–566
- Torri R, Oshima M, Kobayashi T, Takagi K, Tezduyar T (2007a) Influence of wall elasticity in patient-specific hemodynamic simulations. *Computers and Fluids* 36:160–168
- Torri R, Oshima M, Kobayashi T, Takagi K, Tezduyar T (2007b) Numerical investigation of the effect of hypertensive blood pressure on cerebral aneurysm dependence of the effect on the aneurysm shape. *International Journal for Numerical Methods in Fluids* 54:995–1009
- Turek S (1999) *Efficient Solvers for Incompressible Flow Problems: An Algorithmic and Computational Approach*. Springer-Verlag
- Turek S, Schmachtl R (2002) Fully coupled and operator-splitting approaches for natural convection flows in enclosures. *International Journal for Numerical Methods in Fluids* 40:1109–1119
- Valencia A, Ladermann D, Rivera R, Bravo E, Galvez M (2008) Blood flow dynamics and fluid–structure interaction in patient -specific bifurcating cerebral aneurysms. *International Journal for Numerical Methods in Fluids*

58:1081–1100

Vanka SP (1985) Implicit multigrid solutions of Navier-Stokes equations in primitive variables. *J of Comp Phys* 65:138–158

Wheeler D, Chappey C, Lash A, Leipe D, Madden T, Schuler G, Tatusova T, Rapp B (2000) Database resources of the national center for biotechnology information. *Nucleic Acids Res* 28:10–14